



Positron Scattering from Pyrimidine

Abhishek Prashant¹, Meetu Luthra¹, Kanupriya Goswami² , Anand Bharadvaja^{1,*}  and Kasturi Lal Baluja³

¹ Department of Physics, Bhaskaracharya College of Applied Sciences, University of Delhi, New Delhi 110075, India

² Department of Physics, Keshav Mahavidyalaya, University of Delhi, Delhi 110034, India

³ Formerly at Department of Physics and Astrophysics, University of Delhi, Delhi 110007, India

* Correspondence: anand_bharadvaja@yahoo.com

Abstract: The positron impact cross-sections of pyrimidine molecules are reported from 1 eV to 5000 eV. These cross-sections include differential elastic, integral elastic, and direct ionisation. The elastic cross-sections are computed using the single-centre expansion scheme whereas the direct ionisation cross-sections are obtained using the binary-encounter-Bethe formula. The integral and differential cross-sections exhibit consistency with the experimental and other theoretical results. The direct ionisation cross-sections, which are reported for the first time, are compared with the experimental inelastic cross-sections (the sum of excitation and ionisation) to assess the trends in theoretically computed ionisation cross-sections and with the corresponding results for the electrons. The incoherently summed elastic and ionisation cross-sections match very well with the total cross-sections after 40 eV indicating the minimal impact of the positronium formation and electronic excitation processes. Based on this study, we recommend that the experimental data of the inelastic cross-sections reported by Palihawadana et al. be revisited.

Keywords: positron collision; cross-sections; BEB model; single-centre expansion method; close-coupling methods; positronium



Citation: Prashant, A.; Luthra, M.; Goswami, K.; Bharadvaja, A.; Baluja, K.L. Positron Scattering from Pyrimidine. *Atoms* **2023**, *11*, 55. <https://doi.org/10.3390/atoms11030055>

Academic Editors: Dhanoj Gupta, Suvam Singh and Paresh Modak

Received: 12 February 2023

Revised: 6 March 2023

Accepted: 9 March 2023

Published: 10 March 2023



Copyright: © 2023 by the authors. Licensee MDPI, Basel, Switzerland. This article is an open access article distributed under the terms and conditions of the Creative Commons Attribution (CC BY) license (<https://creativecommons.org/licenses/by/4.0/>).

1. Introduction

The interaction of charged particles with biomolecules has been the subject of several studies in fields such as applied physics, technology development, and medicine [1–5]. Positron technology is used in positron emission tomography [6,7], diagnostics, and medical treatments [8–12].

The ionisation process is one of the prime mechanisms for generating low-energy secondary electrons and is also responsible for the damage caused to biomolecules upon its interaction with radiation [13]. Similar to low-energy electrons [14], the energetic positrons or the gamma rays produced during positron–electron annihilation may also damage DNA [4,15,16]. A controlled radiation-induced chemical process in the biological systems would yield favourable improvements in radiotherapeutic treatments and minimise damage to the surrounding healthy tissue. This requires an in-depth understanding of the processes involving primary and secondary particles and biomolecules [17]. The interactions between a projectile and its target are studied in terms of the cross-sections as a function of the energy. Thus, the modelling process essentially means the computation of scattering cross-sections. The positron scattering cross-sections are the essential input in Monte Carlo simulation-based particle tracking codes [4]. Apart from the interaction between a positron and the biomolecules, the positron scattering is equally relevant in astrophysics [18,19], material sciences [20,21], positron plasmas [22], and the transport phenomenon in biological media [23–25].

A complete modelling of a positron–molecule scattering over a wide energy range must include the formation of the positronium ion (Ps), a description of both the bound and continuum states of the target, and the Ps ion. This modelling is sensitive to the

form of polarisation potential in the absence of exchange effects. These factors make the modelling of a positron–molecule scattering more complicated and challenging than that of its antiparticle electron. Ab initio methods, such as the convergent close-coupling method (CCC), the R-matrix with pseudo-states, or the Kohn-Sham method, are complex and require significant resources to compute the cross-sections [26,27]. Even with the latest technology, the computation of the cross-sections for multicentred targets with a large number of electrons may become intractable.

Pyrimidine is an extremely important biomolecule. It is also a precursor for nucleobases, such as cytosine, thymine, and uracil. Structurally, it is an aromatic, heterocyclic, organic compound with the chemical formula $C_4H_4N_2$ and is similar to pyridine. The reactions involving nucleobases are equally important in other fields [28]. This study, therefore, represents a prototype system for investigating positron interactions with DNA and RNA constituents.

Luckily, in the low energy range (below the ionisation threshold), positron–pyrimidine interactions have been studied using the ab initio methods [12,29], whereas, in the energy region beyond the ionisation threshold, methods based on the independent atom model (IAM) [30] have been applied. The IAM is best suited only at higher energies (generally above 100 eV) as the effects due to multiple scatterings between atoms within the molecule are ignored [31,32]. Sanz et al. have applied the R-matrix theory [27,33] and the screening-corrected additivity rule (IAM-SCAR) to different energy ranges [34,35] to study the positron–pyrimidine scattering [29]. Franz and Gianturco [36] have computed integral and differential elastic cross-sections by employing model correlation–polarisation potentials of up to 20 eV, whereas Barbosa et al. [12] employed the Schwinger multichannel method to compute the scattering observables. In these results, the Born correction [37,38] was applied to include the long-range effects due to the polar nature of the target. Studies have also been performed by Singh et al. [30] over an extended energy range.

The machines employed at the University of Trento and the Australian National University (ANU) to perform scattering experiments are based on retarding the potential technique. The linear transmission-type spectrometer at the University of Trento utilises the beam intensity attenuation technique [39] to measure positron and electron scattering from atoms and molecules. This instrument has an energy resolution of a few tenths of an eV. The ANU transmission-type spectrometers are based on the Surko trap system [40] in which the positron beam is formed in a strong magnetic field. This setup is described in detail by Sullivan et al. [41]. The angular discrimination values (the minimum or critical value below which the elastically scattered positrons cannot be distinguished from the incident positrons) of both of these machines compare favourably with each other. More precisely, the angular discrimination values of the ANU spectrometers are slightly lower than that of the University of Trento machines because of the stronger magnetic fields applied. The experimental measurements of the elastic and total cross-sections performed using purely electrostatic, or the more traditional electrostatic and magnetic field-type, spectrometers always suffer from the angular discrimination effects of the equipment. These effects contribute significantly to scattering measurements at low energies for a polar target. The experimental data must, therefore, be corrected to draw comparisons with the theoretical data; otherwise, the experimental results will always be underestimated [42]. This issue is also dealt with in the present work. Zecca et al. [43] performed an experiment at the University of Trento at a retarding potential of 90 mV. Palihawadana et al. [44] have measured the elastic cross-section at a retarding potential of 378 mV whereas, in the data set obtained from the difference between the grand total cross-section and the cross-sections for positronium formation and ionisation, the retarding potential was 72.8 mV. The values of the total cross-sections reported by Palihawadana et al. [44] are higher than those reported by Zecca et al. [43] due to differences in the angular resolution of the two experiments. The theoretical and experimental studies on positron scattering from pyrimidine have been summarised by Brunger et al. [45].

In the present work, we compute cross-sections from low to high energy ranges by considering the molecular approach, that is, we do not apply the additivity rule to compute cross-sections. The method is discussed in the next section. Since, the ab initio methods require a lot of expertise, a simple treatment to model the scattering process for multi-electron polyatomic molecules is required. One of the most convenient approaches to modelling the scattering phenomenon is to compute the cross-sections corresponding to different processes by neglecting inter-channel coupling and employing different methodologies. These cross-sections can then be summed incoherently to estimate the total cross-sections. For example, the elastic scattering can be modelled using optical potentials [46–48], the direct ionisation cross-sections can be computed with the binary-encounter-Bethe approximation (BEB) [49], and the dipole-allowed electronic excitation process with a binary approximation [50]. This approach simplifies the modelling phenomena and makes the calculations tractable at large energies. This also helps to reduce the computational cost significantly. On the other hand, the ab initio methods may make the calculations intractable due to the accessibility of a large number of channels at large energies.

The integral elastic and differential cross-sections (DCS) at different energies are reported by applying the symmetry-adapted single-centre expansion (SCE) technique [51,52] within the local potential approximation. The correction to the differential and integral cross-sections is accounted for via the Born closure technique [48,53]. The direct ionisation cross-sections are estimated using the binary-encounter-Bethe (BEB) model for positrons [49]. Since methods for modelling positronium formation (Ps) do not exist, these cross-sections were not considered. The cross-sections obtained from the incoherent sum of the elastic and BEB cross-sections show a good agreement with the experimental data beyond 40 eV. All results reported here show consistency with the previously determined results.

This paper is organised as follows: In Section 2, we describe the theoretical model for computing integral elastic cross-sections (ECS) and ionisation cross-sections. In Sections 3 and 4, we present the computational details and the results. Toward the end, in Section 5, we present our conclusions.

2. The Single-Centre Expansion Method and the Binary-Encounter-Bethe Model

2.1. Elastic Cross-Sections

The positron (or electron)–target collision in the symmetry-adapted single-centre expansion method is described in terms of the effective one-particle interaction potentials. This method involves a single-centre expansion of a quantity such as the potential, bound state, or scattering wave function around the centre of mass (c.o.m.) of the projectile–molecule system [52]. This simplifies the quantum scattering equations [54,55]. A single-determinant Hartree–Fock approach is used to represent the wave function of the present target. This implies that the excited states are excluded from the description of the total wave function. In simple terms, it means that the wave function is described by the ground state of the target. The static potential (V_{st}) is repulsive in positron scattering and describes the electrostatic interaction between the undeformed molecular charge distribution of the target and the projectile. The correlation and polarisation potential (V_{cp}) consists of long- and short-range regions that are matched at a particular distance (r_c). The behaviour of V_{cp} is represented as:

$$V_{cp}(\vec{r}) = \begin{cases} V_{corr}(\vec{r}) & \text{for } r \leq r_c \\ V_{pol}(\vec{r}) & \text{for } r > r_c, \end{cases} \quad (1)$$

The model potential given by Perdew and Zunger [56] is used in the present calculations to represent V_{corr} . The total interacting potential $V(r)$ is the sum of V_{st} and V_{cp} , as the exchange effects are absent.

In SCE, the potential (total V_{st} or V_{cp}) in its expanded form can be written in terms of the symmetry-adapted angular functions $X_{lh}^{p\mu}(\theta, \phi)$ as:

$$V(\vec{r}) = \sum_{lm} V_{lm}(r) X_{lm}^{p\mu}(\theta, \phi), \tag{2}$$

Similarly, the bound-state wave function is given by:

$$u_i(\vec{r}) = \frac{1}{r} \sum_{l,h} u_{i,hl}(r) X_{hl}^{p\mu}(\theta, \phi), \tag{3}$$

where μ describes the p th irreducible representation (IR) for a point group, h is the particular basis for a given partial wave l for μ , i is the specific multicentre orbital contributing to the density of the bound electrons, r is the distance from the c.o.m. of the molecule, and $u_{i,hl}$ is the radial coefficient. The $X_{lh}^{p\mu}(\theta, \phi)$ are given by a linear combination of the spherical harmonics $S_{lm}(\theta, \phi)$:

$$X_{lh}^{p\mu}(\theta, \phi) = \sum_{m=-l}^{+l} b_{lhm}^{p\mu} S_{lm}(\theta, \phi). \tag{4}$$

The IR-dependent coefficients b_{lhm} are given by the character table [57]. The Schrödinger equation describing the scattering in terms of its partial waves is given by:

$$\left[\frac{d^2}{dr^2} - \frac{l(l+1)}{r^2} + k^2 \right] \psi_{lh}^{p\mu}(r) = 2 \sum_{l'h'} V_{lh, l'h'}^{A_1}(r) \psi_{l'h'}^{p\mu}(r), \tag{5}$$

where $k^2/2$ is the collision energy, and $\psi_{l'h'}^{p\mu}(r)$ are the radial continuum wave functions of the positron. The local potential coupling element $V_{lh, l'h'}^{A_1}(r)$ is given by:

$$V_{lh, l'h'}^{A_1}(r) = \int d\hat{r} X_{lh}^{p\mu}(\hat{r}) V(\vec{r}) X_{l'h'}^{p\mu}(\hat{r}). \tag{6}$$

Finally, the elastic cross-sections are extracted from the T -matrix elements in the body-fixed frame (BF) after solving the Schrödinger equation:

$$\sigma_e^{BF} = \frac{\pi}{k^2} \sum_{lh} \sum_{l'h'} |T_{lh, l'h'}|^2. \tag{7}$$

The BF elastic cross-sections were then Born corrected [37] via the Born top-up formula [48,53].

$$Q_e^{BF} = \sigma_e^{BF} + \delta^B, \tag{8}$$

where

$$\delta^B = Q^B - Q_L^B. \tag{9}$$

The Born correction term δ^B is defined as the difference between the Born cross-sections (Q^B) and the cross-sections obtained for L partial waves with in the Born formalism (Q_L^B).

The DCS of the polar molecules are determined in the LAB frame (LF) by applying the frame transformation [58]. This avoids the diverging nature of DCS due to a singularity in the forward direction with in the fixed nuclei approximation (FNA). A closure formula helps obtain the converged DCS [37,38] in LF:

$$\frac{d\sigma}{d\Omega}(J\tau \rightarrow J'\tau') = \frac{d\sigma^B}{d\Omega}(J\tau \rightarrow J'\tau') + \sum_{L=0}^{L_{max}} (A_L(J\tau \rightarrow J'\tau') - A_L^B(J\tau \rightarrow J'\tau')) P_L(\cos\theta), \tag{10}$$

where $P_L(\cos\theta)$ is a Legendre polynomial, and A_L is the scattering coefficient [57]. L_{max} represents the maximum number of partial waves included in the scattering calculations. The first term represents the DCS obtained for a rotating dipole, and the second term

denotes the DCS calculated for a fixed dipole within the first Born approximation. $J\tau$ and J', τ' are the initial and final rotational levels. In Born-approximated terms, $J' = 1$, and $\tau' = 0$.

The corresponding integral cross-sections in the LF are given by:

$$Q_e^{LF} = \sigma_{e,rd}^B + \sigma_e^{BF} - \sigma_{e,fd}^B \quad (11)$$

Equations (10) and (11) thus include both the long- and short-range effects (from the BF calculations). The rotationally unresolved DCS are obtained after summing the DCS over the final rotor state ($J'\tau'$).

2.2. Direct Ionisation Cross-Sections

An ab initio description of positron scattering is a two-centre close-coupling (CC) method in which the wave function of the scattering system is expanded over the target and Ps eigenstates [26,59,60]. Although CC methods are capable of calculating the total ionisation cross-sections (TICS) accurately, these methods are not user-friendly. Moreover, these methods require enormous computational resources, thus making calculations costly and expensive. Additionally, these methods are difficult to apply to complex molecular systems. In comparison, a semi-empirical method, such as the BEB model for positrons [49], is extremely simple both in its formulation and workings. It computes the total ionisation cross-sections over an extensive energy range quickly even for complex molecular targets. In fact, the ionisation cross-sections obtained for H_2 using the BEB model [49] have shown a high degree of consistency with the two-centre expansion scattering calculations employing the molecular CCC model [61]. These ab initio calculations are the benchmark calculations performed for the ionisation of H_2 due to positrons thus far. The total ionisation cross-sections (TICS) in the BEB model are obtained after summing the cross-sections over the N occupied molecular orbitals [49]:

$$Q_i^{e^+}(t_i) = \frac{S}{t_i + \gamma} \left[\frac{Q}{2} \left(1 - \frac{1}{t_i^2} \right) \ln t_i + (2 - Q) \left(1 - \frac{1}{t_i} \right) \right], \quad (12)$$

where

$$\gamma = u + 1 + \frac{C}{(t_i - 1)^{1.65}}, \quad (13)$$

The TICS are therefore:

$$Q_I(t) = \sum_i^N Q_i^{e^+}(t_i). \quad (14)$$

Here, $t_i = E/B_i$, $u_i = U_i/B_i$, and $S = 4\pi a_0^2 N_i (R/B_i)^2$. R, B_i, U_i , and N_i refer to the Rydberg energy, the binding energy, the orbital kinetic energy, and the orbital occupation number, respectively, of the i th orbital; a_0 is the Bohr's radius. The scaling term $t_i + \gamma$ ensures the validity of the Wannier law for positrons [62] near the threshold. The constant C is normally taken as unity; however, its exact value can be derived for a target only if reliable positron cross-sections are available [49]. The value of $Q = 1$ makes the BEB model independent of the differential oscillator strengths [63].

3. Computational Details

The optimised geometry of pyrimidine was referred from NIST [64] corresponding to the cc-pVTZ basis. Its ground-state electronic configuration corresponds to the 1A_1 symmetry in the C_{2v} point group. The Gaussian software [65] was used to generate the input parameters for the BEB model at the optimised geometry. The use of experimental values of the ionisation energy (IE) ensured the correct threshold behaviour of the TICS. $S_{lm}(\theta, \phi)$ was constructed as a sum over a single index lm , with $h = 1$, and $p\mu$ equals A_1 as pyrimidine is a closed-shell non-linear molecule. The one-particle electron density and the potentials were obtained using the SCELiB code at the HF level [66]. The experimental

value of the polarisability was referred to in order to compute V_{cp} . The maximum value of l , i.e., l_{max} , used in the expansion of bound-state molecular properties, was taken as 48. The radial step size for integration was taken as 0.005 au. The large value of l ensured that all orbitals were either normalised to unity or were close to unity. The dipole moment obtained from the numerical SCE wave function matched well with its experimental value. The values of the dipole moment obtained from the numerical SCE wave function and the other target parameters needed to perform scattering calculations are listed in Table 1. The scattering calculations were completed using the POLYDCS code [67]. This code yields Born-corrected cross-sections. The corrections to the BF cross-sections were also applied directly via the Born top-up programme. The experimental value of the dipole moment was used to compute the corrections.

Table 1. Experimental values of a few important target parameters of pyrimidine. The SCE value of the dipole moment is also shown.

Ionisation Energy	Ps	Dipole	Polarisability	Lowest Excitation Threshold
9.33 eV [64]	2.53 eV	2.28–2.4 D [68] 2.37 D (SCE)	60 au [43]	4 eV [69]

4. Results

The positron impact cross-sections are reported for various processes over a wide energy range. The DCS are presented first, followed by the integral ECS, and then the ionisation cross-sections. A comparative evaluation of the present and other existing results is also performed. The angular discrimination effect of the linear transmission-type spectrometer used to measure cross-sections is also discussed.

The Born-corrected DCS are plotted in Figure 1a–g at different incident energies. These are precisely peaked in the forward direction due to the cumulative effect of the large value of the dipole moment and the dipole polarisability. At large angles, the magnitude of the cross-sections is small, indicating the dominating nature of backward scattering. At incident energies of 6, 10, 15, and 20 eV (and higher), we have shown the DCS without Born correction, that is, these results do not include the dipole contributions. At 3 eV, the DCS calculated from the pure Born approximation are reasonably close to the experimental values. This is because of the large dipole moment of pyrimidine. The deviations between the corrected and uncorrected DCS are large at lower energies and in the angular range of 0–40°. At 100 eV, the angular deviations become confined to a narrow angular range. This indicates the diminishing effect of the dipole moment on scattering as the incident energy of the projectile increases. The DCS curves are smooth at lower energies but exhibit oscillatory behaviour at higher energies (above 10 eV). The undue oscillations arise after applying the Born closure approach to include the long-range effects and are attributed to the incomplete convergence of higher partial waves, accounting for the dipole potential term $A_L^B P_L(\cos\theta)$ in the Born closure method. These oscillations have been observed in several studies performed earlier [36,48,70–73]. The Born closure approach can also give unphysical results [38]; however, this situation was avoided by carefully choosing the input parameters in POLYDCS. Palihawadana et al. [44] have previously reported the folded DCS [74] from 12–87°. These results were also recommended by Brunger et al. [45]. Sanz et al. [29] have also computed the theoretical DCS using the additivity rule by considering the dipole potential (V_d) and the dipole-plus-quadrupole potential (V_{d+q}). The Dickinson correction [75] was applied to the DCS. Barbosa et al. [12] have reported the elastic integral and differential cross-sections at incident energies of up to 20 eV using the Schwinger multichannel method. The elastic cross-sections were Born corrected following the Born closure procedure. We have compared the present SCE-DCS with all these data. Our results lie within the uncertainty range of the experimental results.

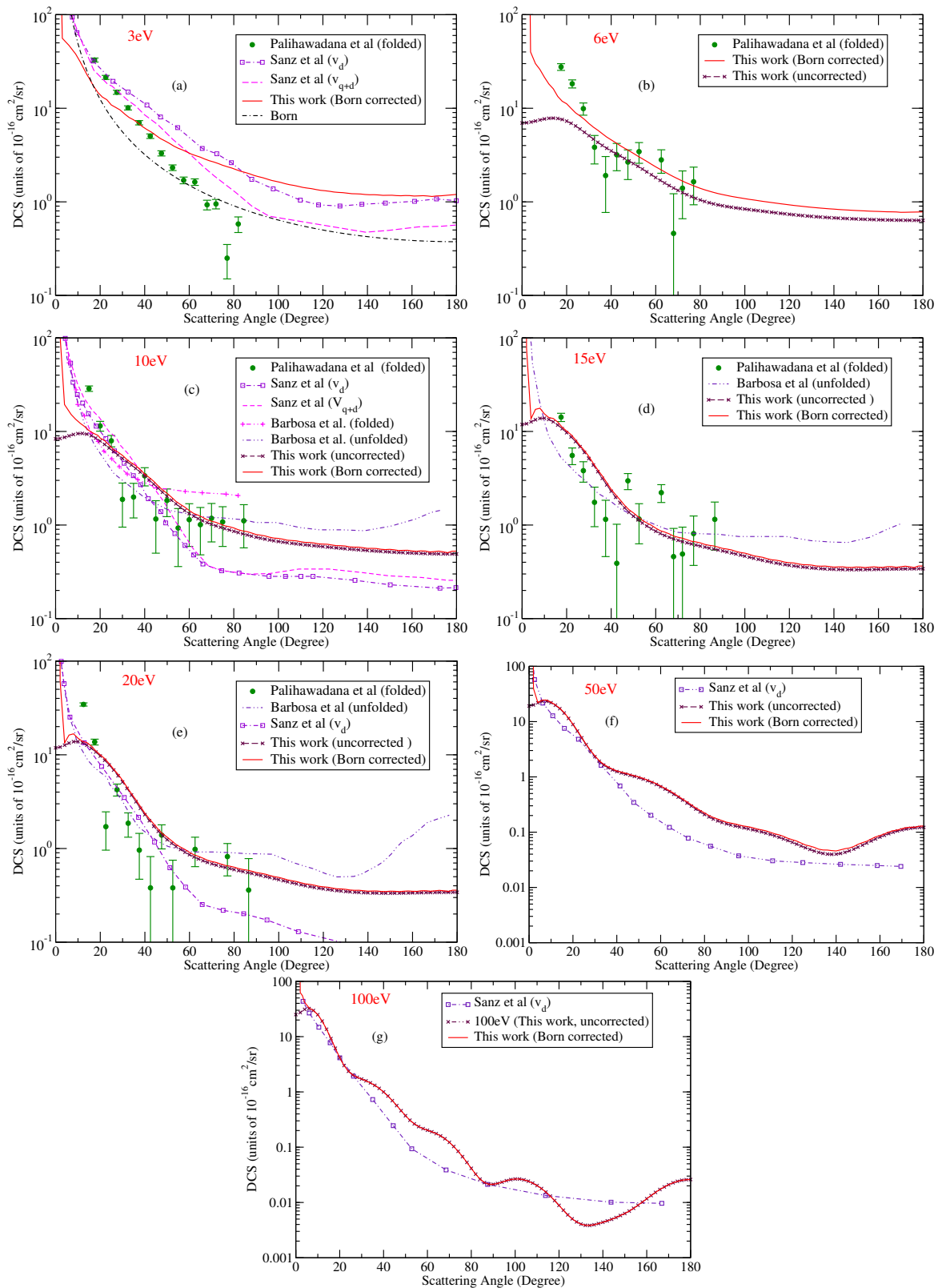


Figure 1. DCS at different energies: circles, folded DCS of Paliwadana et al. [44]; line curve, Born-corrected DCS (this work); dashed dotted curve, Born cross-sections; open squares with dotted dashed curve, Sanz et al. with dipole potential [29]; dashed curve, Sanz et al. with dipole and quadrupole potentials [29]; dashed curve with cross, DCS results without Born correction; double dotted dashed curve, unfolded DCS of Barbosa et al. [12]. Their folded DCS are shown as a double dotted dashed curve with plus symbol.

We also see a good agreement with the other theoretical data. The difference between the present and other results appears large as the graphs are plotted on a log scale. The experimental DCS results are available up to 20 eV only.

The integral elastic cross-sections in the BF and LAB frames were computed using the POLYDCS code. The BF results were without the dipole correction. We adopted two different schemes to carry out these corrections. The Born correction was applied directly to the BF elastic results via the Born top-up formula. We also used the POLYDCS code to obtain the Born-corrected data. We did not notice any meaningful deviations in the corrections from the two approaches. The integral cross-sections increase as the incident energy decreases. The sharp rise in the low incident energies is attributed to the Born correction, which significantly raises the magnitude of the cross-sections. The lower ECS results of Palihawadana et al. [44] are due to the angular discrimination effects of the spectrometer. The experimental elastic cross-section measurements of Palihawadana et al. [44] were corrected using the critical data from their spectrometer with the Born top-up formula [48]. This significantly increased the magnitude of the cross-sections. A good agreement between the Born-corrected SCE and the forward-angle-corrected experimental data can be observed from Figure 2b while considering the simplicity of the approach. This agreement improves further as the energy of incoming positron increases. It is mentioned here that Franz and Gianturco [36] used a similar approach but did their calculations using the DFT theory and a different basis set. This accounts for the difference between our results and their results. However, for sake of clarity, we have not shown their results. The impact of the Born correction is quite large at low energies and extends up to higher values due to the large value of the dipole moment. The merging between the corrected and uncorrected results is after 200 eV.

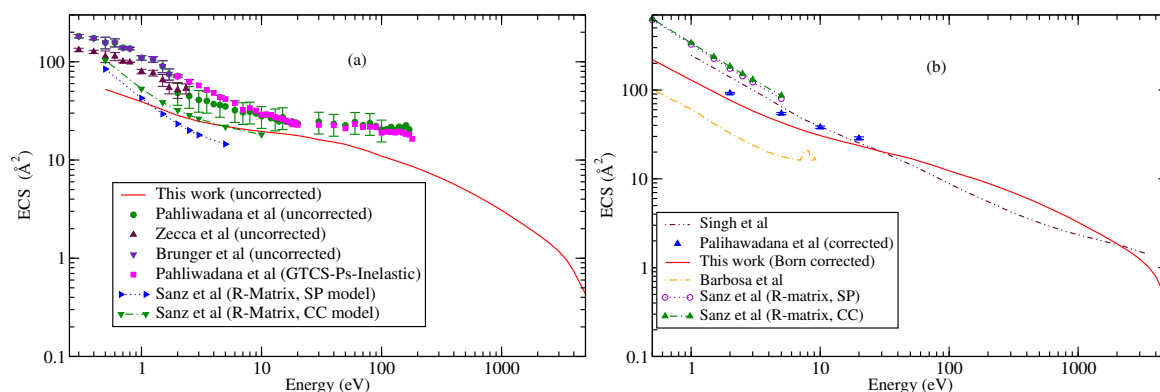


Figure 2. ECS: (a) Born-uncorrected; (b) Born-corrected. Experimental results are denoted by symbols and the theoretical results by line curves or line curves with symbols. The notation “R-matrix, SP” in (b) stands for “static-polarisation model”. “CC” model means the ground state and excited states included in the total wave function [29,30,43–45].

Sanz et al. have performed low-energy R-matrix calculations in static-exchange and CC models. They have completed the calculations using the IAM-SCAR model from 1 eV to 10 keV [29]. These data were further corrected to account for the polar nature of the molecule. Brunger et al. [45] have recommended the uncorrected forward-angle scattering effect data of Palihawadana et al. [44] at low energies and Zecca et al. at higher energies.

These data do not vary much from the measurements reported by Palihawadana et al. [44]. Since the correction is a typical feature of the equipment used and the target studied, the same correction is valid for the recommended data of Brunger et al. [45]. For this reason, we have not shown the corrected experimental data of Brunger et al. [45] in Figure 2b. Zecca et al. have not given the critical data of their instrument in their study on pyrimidine [43]. Hence, these data were not corrected. Brunger et al. [45] have given the angular discrimination factors of the spectrometer at the University of Trento. Using this, one can easily correct the experimental data of Zecca et al. [43]. Franz et al. have

shown this in their work [36]. We have also shown that any scattering data obtained using the spectrometer at Trento can be corrected once we know the critical data of the measuring equipment [46,48]. In one of the studies, we have also shown that the University of Trento and the Australian National University have nearly the same values of correction for the cross-sections even though both of these spectrometers have different workings and constructions [48]. The uncorrected and corrected theoretical and experimental elastic cross-sections from 1 eV up to 5 keV are shown in Figure 2a,b, respectively.

The BEB model-based direct ionisation cross-sections are plotted in Figure 3. The maxima in the BEB cross-sections appear at 70 eV and have a magnitude of 13.01 \AA^2 . The high-energy behaviour is dominated by the $\log E/E$ term. Owing to the non-availability of data to compare the present results, we have assessed the trends in the BEB results by comparing them with the inelastic results and ionisation results due to electron impact. Palihawadana et al. [44] have determined the inelastic cross-sections (the sum of both the electronic excitations and ionisation cross-sections) up to 21.5 eV. These results are lower than the BEB results but show rising trends with the incident energy. The ionisation cross-sections rise up to the maximum value, which is in the range of 70–80 eV for most of the molecules, and then decrease. Thus, we expect the rising trends for the summed inelastic cross-sections of Palihawadana et al. [44] after 21.5 eV. The excitation threshold is lower than the ionisation threshold, which means that, in the energy range from 4 eV to 9.33 eV, it is the electronic excitation process that would contribute to the grand total scattering cross-sections. The onset of any inelastic process occurs once the threshold of a particular process has been exceeded. It is, therefore, expected that cross-sections for the excitation process would be zero below 4 eV. On the contrary, the summed inelastic (excitation and ionisation) cross-sections of Palihawadana et al. [44] are non-zero below 4 eV (excitation threshold) and zero at energies of 4–5 eV and 6.5 eV. These values are not consistent with the fundamentals of scattering theory. Unfortunately, we do not have any reason to justify the summed inelastic cross-sections (excitation and direct ionisation) reported by Palihawadana et al. [44] below 7 eV. Even Brunger et al. [45] have not listed the inelastic cross-sections of Palihawadana et al. [44] in their recommended data. This gives us a strong feeling that the inelastic cross-sections of Palihawadana et al. [44] must be reviewed.

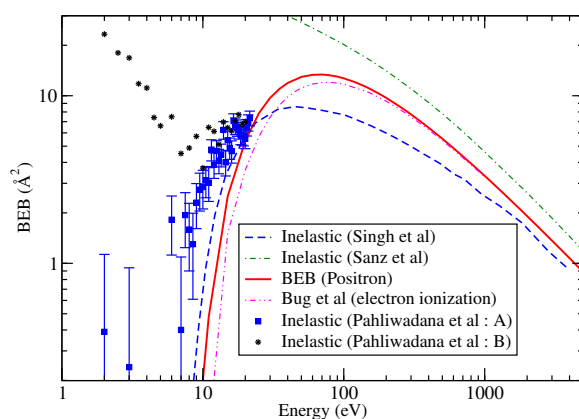


Figure 3. BEB ionisation cross-sections. The comparison is made with inelastic cross-sections (excitation plus ionisation) reported by Palihawadana et al. [44] and ionisation cross-sections due to electron impact. Squares: direct measurements of inelastic cross-sections (excitation plus ionisation) by Palihawadana et al. [44] denoted as A; stars: inelastic cross-sections as a difference of grand total and Ps and elastic cross-sections from Palihawadana et al. [44] denoted as B; line curve: BEB for positron (this work); dashed curve, inelastic cross-sections (excitation plus ionisation) due to positron impact of Singh et al. [30]; dotted dashed curve, positron impact total inelastic cross-sections of Sanz et al. [29]; double dotted dashed curve, electron ionisation of Bug et al. [76].

We further calculated the summed inelastic (excitation and ionisation) cross-sections from the experimental readings of Palihawadana et al. [44] by subtracting the sum of the

ECS and Ps from the grand total results. The two data sets are highly scattered up to 9 eV. Both of the data sets of Palihawadana et al. [44] (direct measurements and from the subtraction of the summed Ps and ECS from the grand total cross-section) converge only after 10 eV. This dispersion in the two data sets can be partly due to the different retarding potentials used to measure the elastic and grand total cross-sections. The fact that the grand total cross-sections contain contributions from all of the possible energetic channels in a given energy range could be another reason explaining this variation in the two data sets.

The positron ionisation results were compared with the electron impact ionisation results of Linert et al. [77], Champion et al. [78], and Bug et al. [76]. The results of Bug et al. [76] and Champion et al. [78] predict higher estimates of the ionisation cross-sections than Linert et al. [77]. The results of Bug et al. [76] are comparable to the BEB model [63] due to electron impact [79]. The BEB model provides higher estimates of the results for positrons [49] than for electrons [63]. This is due to the inclusion of the exchange and interference effects in positron scattering. Additionally, in several cases in which the data are available for both projectiles, it has been observed that the positron impact ionisation cross-sections are always higher than that of the electron impact. The same is also observed in the case of pyrimidine. The overlapping of the trends of both the BEB curves is expected beyond 500 eV, which means the effects arise due to the charge of the projectile ceasing. This gives us the feeling that our BEB results for positrons are acceptable. For the sake of the clarity of the results, we have not shown the electron impact ionisation results of Linert et al. [77] and those computed from the BEB model [79]. This mutual comparison of the results of antiparticles can be used as a tool to ascertain the results in the absence of positron ionisation data.

Ps formation was impossible for us to model theoretically. The elastic and inelastic cross-sections were added in an incoherent fashion to obtain the cross-sections Q_T from 0.5 eV onwards. These results were compared with the forward-angle-corrected experimental results of Palihawadana et al. [44]. For a better understanding and interpretation of the results, we have also shown the recommended data of Brunger et al. [45] and Zecca et al. [43]. We observe that Q_T (obtained after ignoring the Ps and excitation channels) agree well with the experimental data from 40 eV onwards. This is indicative of the fact that these channels are most dominant in the energy region of 2.5 eV–40 eV. The visible disagreement between the present and experimental data at low energies is due to the exclusion of the Ps and excitation channels. Additionally, the lower values of the SCE-ECS add to the variation in this energy range. This has already been discussed above. In the same figure, we have shown the IAM-SCAR calculations by Sanz et al. [29], which were obtained by considering the dipole polarisation and dipole-plus-quadrupole potentials and the results obtained from the complex spherical optical method by Singh et al. [30] using the additivity rule. The results are displayed in Figure 4. The Ps formation is also marked on the graph at 2.53 eV. If we include the Ps data of Palihawadana et al. [44] and add it to our Q_T , the results show a remarkable agreement with the experimentally corrected data of Palihawadana et al. [44].

The lower values of the total cross-sections of Zecca et al. [43] are attributed to the angular discrimination of the experimental apparatus. Overall, one can notice reasonable qualitative conformity in the present results with the corresponding results for the numerous other kinds of processes.

Of course, the present analysis has several limitations, just as the SCeLiB code [66] generates the molecular properties only for closed-shell targets. Hence, the scattering due to open-shell targets cannot be modelled. The BEB model cannot be invoked to model the Ps cross-sections since its formation is not a binary collision [80]. Unfortunately, simpler theoretical methods do not exist to model positronium formation. Theoretically, the Ps cross-sections are largely estimated using the phenomenological model proposed by Chiari et al. [81]. However, this approach does not fit into our model.

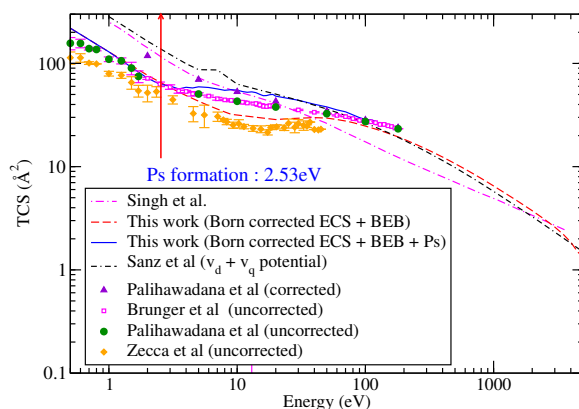


Figure 4. TCS: line curve, this work (sum of ECS+Ps+BEB); dashed curves, this work (sum of ECS+BEB); dashed dotted curve, Sanz et al. [29]; dotted dashed curve, Singh et al. [30]; diamonds, uncorrected TCS of Zecca et al. [43]; circles, uncorrected results of Palihawadana et al. [44]; squares, recommended data of Brunger et al. [45]; triangles, forward-angle-corrected TCS of Palihawadana et al. [44].

Another limitation is that we have ignored the inter-channel coupling, which does impact the cross-section data. However, in the case of pyrimidine, the vibration and rotational cross-sections are very small in magnitude in comparison to the elastic or ionisation cross-sections at the energies considered by Palihawadana et al. [44]. Thus, the impact of these channels on the total scattering cross-sections would not be too large.

The theoretical quantum scattering-based models, or models employing quantum mechanically generated data, provide an effective tool for deriving cross-sections. Additionally, these methods yield information about scattering observables that cannot be determined experimentally. For example, the cross-sections below certain energies and angles cannot be measured experimentally for polar targets [42,45]. This means that the experimentally measured cross-sections for polar molecules are always lower than the true values. Their true values can only be estimated theoretically by applying some correction to the existing data. This correction depends on the strength of the dipole moment and can be substantive at low energies for strongly polar molecules [45]. We, therefore, need theoretical methods not only to validate the experimental data but also to estimate the collision data at other energies. Similarly, the theoretical results also need a correction to account for the long-range nature of the polar targets. Thus, correction must be properly accounted for in both the theoretical and experimental results before drawing any meaningful comparison between the two.

Although the ab initio methods provide excellent results, this happens at a considerable cost to the computation. Additionally, the complexity of the calculations grows with the number of electrons in these methods and with an increase in the incident energy of the projectile. These ab initio calculations may also suffer from issues such as ill-conditioning [26,59,60] or linear dependence [27]. Thus, we require alternate methods and a simplified approach to circumvent this problem in order to compute cross-sections. This is what we have shown in the present work without invoking the independent atom model (IAM) approximation.

5. Conclusions

This paper has reported various types of cross-sections for positron–pyrimidine interactions from low to high energies in a very simple and efficient manner. This approach is particularly helpful in performing scattering studies involving many-electron molecular systems that consist of a large number of atoms. In such systems, the perturbative methods may become intractable. For the reasons stated in this manuscript, the direct ionisation cross-sections are difficult to measure and compute. It is equally true that the positron

impact inelastic cross-sections (excitation, ionisation) with pyrimidine are relevant for radiation-based biomedical applications as these lead to the formation of new species. Thus, it is necessary to have a broad database of inelastic cross-sections. The BEB method provides an opportunity to estimate ionisation cross-sections. These data have not been reported in earlier studies. The comparison with electron scattering provides useful insight into the scattering process. While electron ionisation mass spectrometry data are available for a large number of molecules, positron ionisation mass spectrometry data are not. Once these are available, it would be interesting to modify the BEB model for positrons to compute the partial ionisation cross-sections of a molecule and compare these with the corresponding experimental data. The modified BEB model has shown promising results for the large number of cations formed due to electron impact ionisation for simple as well as complex targets [82,83]. The studies have shown that the Born top-up programme can be used to correct the experimental data of the TCS and ECS at any energy without relying on the DCS. We are unable to address trends in the experimental results for the inelastic process due to positron impact up to 7 eV. We expect the present results will surely be of help for future investigations.

Author Contributions: Conceptualization, supervision, and methodology, K.L.B. and A.B.; original calculations and draft, A.P.; review, calculation checking, redrafting, and editing, M.L., A.P. and K.G. All authors have contributed equally to this work. All authors have read and agreed to the published version of the manuscript.

Funding: This research received no external funding.

Institutional Review Board Statement: Not applicable.

Informed Consent Statement: Not applicable.

Data Availability Statement: The data may be obtained from the authors upon request.

Conflicts of Interest: The authors declare no conflict of interest.

Abbreviations

The following abbreviations are used in this manuscript:

SCE	Single-Centre Expansion
ECS	Elastic Cross-Sections
DCS	Differential Cross-Sections
TCS	Total Cross-Sections
TICS	Total Ionisation Cross-Sections
IE	Ionisation Energy
BEB	Binary–Encounter–Bethe
HF	Hartree–Fock
DFT	Density Functional Theory
IE	Ionisation Energy
CC	Close-Coupling
eV	Electron Volt
au	Atomic Unit
IAM	Independent Atom Approximation

References

1. Cherry, S.R.; Sorenson, J.A.; Phelps, M.E. *Physics in Nuclear Medicine*, 4th ed.; Elsevier: Philadelphia, PA, USA, 2012.
2. Jaini, S.; Dadachova, E. FDG for Therapy of Metabolically Active Tumors. *Nucl. Med.* **2012**, *42*, 185. [[CrossRef](#)] [[PubMed](#)]
3. Nikjoo, H.; Taleei, R.; Liamsuwan, T.; Liljequist, D.; Emfietzoglou, D. Perspectives in radiation biophysics: From radiation track structure simulation to mechanistic models of DNA damage and repair. *Radiat. Phys. Chem.* **2016**, *128*, 3–10. [[CrossRef](#)]
4. Tejedor Gomez, G.G.; Fuss, M.C. *Radiation Damage in Biomolecular Systems*; Springer: Berlin, Germany, 2012.
5. Surko, C.M.; Gianturco, F.A. (Eds.) *New Directions in Antimatter Chemistry and Physics*; Kluwer Academic Publishers: Dordrecht, The Netherlands, 2001.

6. Wahl, R.L.; Buchanan, J.W. *Principles and Practice of Positron Emission Tomography*; Lippincott, Williams and Wilkins: Philadelphia, PA, USA, 2002.
7. Bailey, D.; Townsend, W.; Valk, P.; Maisey, M. *Positron Emission Tomography*; Springer: London, UK, 2005.
8. Müller, H.; Enghardt, W. In-beam PET at high-energy photon beams: A feasibility study. *Phys. Med. Biol.* **2006**, *51*, 1779. [[CrossRef](#)] [[PubMed](#)]
9. Pshenichnov, I.; Mishustin, I.; Greiner, W. Distributions of positron-emitting nuclei in proton and carbon-ion therapy studied with GEANT4. *Phys. Med. Biol.* **2006**, *51*, 6099. [[CrossRef](#)]
10. Moadel, R.M.; Weldon, R.H.; Katz, E.B.; Lu, P.; Mani, J.; Stahl, M.; Blaufox, M.D.; Pestell, R.G.; Charron, M.J.; Dadachova, E. Positherapy: Targeted Nuclear Therapy of Breast Cancer with 18F-2-Deoxy-2-Fluoro-D-Glucose. *Can. Res.* **2005**, *65*, 698–702. [[CrossRef](#)][[PubMed](#)]
11. Dijkers, E.C.; Oude Munnink, T.H.; Kosterink, J.G.; Brouwers, A.H.; Jager, P.L.; de Jong, J.R.; van Dongen, G.A.; Schröder, C.P.; Lub-de Hooge, M.N.; de Vries, E.G. Biodistribution of ⁸⁹Zr-trastuzumab and PET Imaging of HER2-Positive Lesions in Patients with Metastatic Breast Cancer. *Clin. Pharmacol. Ther.* **2010**, *87*, 586–592. [[CrossRef](#)]
12. Barbosa, S.A.; Pastega, D.F.; Bettegaa, H.F.M. Low-energy positron scattering by pyrimidine. *J. Chem. Phys.* **2015**, *143*, 244316. [[CrossRef](#)]
13. Boudaïffa, B.; Cloutier, P.; Hunting, D.; Huels, M.A.; Sanche, L. Resonant Formation of DNA Strand Breaks by Low-Energy (3 to 20 eV) Electrons. *Science* **2000**, *287*, 1658–1660. [[CrossRef](#)]
14. Sanche, L. Nanoscopic aspects of radiobiological damage: Fragmentation induced by secondary low-energy electrons, Mass Spectrom. *Mass Spectr. Rev.* **2002**, *21*, 349–369. [[CrossRef](#)]
15. Turi, L.; Rossly, P.J. Theoretical studies of spectroscopy and dynamics of hydrated electrons. *Chem. Rev.* **2012**, *112*, 5641–5674. [[CrossRef](#)]
16. von Sonntag, C. *Free-Radical-Induced DNA Damage and Its Repair*; Springer: New York, NY, USA, 2005; pp. 357–482. [[CrossRef](#)]
17. Sanche, L. Beyond radical thinking. *Nature* **2009**, *461*, 358–359. [[CrossRef](#)] [[PubMed](#)]
18. De Sarkar, A.; Biswas, S.; Gupta, N. Positron excess from cosmic ray interactions in galactic molecular clouds. *J. High Energy Astrophys.* **2021**, *29*, 1–18. [[CrossRef](#)]
19. Guessoum, N. Positron astrophysics and areas of relation to low-energy positron physics. *Euro. Phys. J. D* **2014**, *68*, 137. [[CrossRef](#)]
20. Hulet, L.D., Jr.; Donohue, D.L.; Xu, J.; Lewis, T.A.; McLuckey, S.A.; Glish, G.L. Mass spectrometry studies of the ionization of organic molecules by low-energy positrons. *Chem. Phys. Lett.* **1993**, *216*, 236–240. [[CrossRef](#)]
21. Schultz, P.J.; Lynn, K.G. Interaction of positron beams with surfaces, thin films, and interfaces. *Rev. Mod. Phys.* **1988**, *60*, 701. [[CrossRef](#)]
22. Sarri, G.; Poder, K.; Cole, J.M.; Schumaker, W.; Di Piazza, A.; Reville, B.; Zepf, M.; Mangles, S.P.D.; Najmudin, Z.; Shukla, N.; et al. Generation of neutral and high-density electron–positron pair plasmas in the laboratory. *Nat. Commun.* **2015**, *6*, 6747. [[CrossRef](#)]
23. Sanz, A.G.; Fuss, M.C.; Muñoz, A.; Blanco, F.; Limão-Vieira, P.; Brunger, M.J.; Buckman, S.J.; García, G. Modelling low energy electron and positron tracks for biomedical applications. *Int. J. Radiat. Biol.* **2012**, *88*, 71. [[CrossRef](#)]
24. Blanco, F.; Roldán, A.M.; Krupa, K.; McEachran, R.P.; White, R.D.; Marjanović, S.; García, G. Scattering data for modelling positron tracks in gaseous and liquid water. *J. Phys. B At. Mol. Opt. Phys.* **2016**, *49*, 145001. [[CrossRef](#)]
25. Blanco, F.; Muñoz, A.; Almeida, D.; Silva, F.; Limão-Vieira, P.; Fuss, M.C.; Sanz, A.G.; García, G. Modelling low energy electron and positron tracks in biologically relevant media. *Eur. Phys. J. D* **2013**, *67*, 199. [[CrossRef](#)]
26. Zammit, M.C.; Fursa, D.V.; Savage, J.S.; Bray, I. Electron–and positron–molecule scattering: Development of the molecular convergent close-coupling method. *J. Phys. B At. Mol. Opt. Phys.* **2017**, *50*, 123001. [[CrossRef](#)]
27. Tennyson, J. Electron–molecule collision calculations using the R-matrix method. *Phys. Rep.* **2010**, *491*, 29–76. [[CrossRef](#)]
28. Stryer, L. *Biochemistry*; W. H. Freeman: New York, NY, USA, 1995.
29. Sanz, A.G.; Fuss, M.C.; Blanco, F.; Mašin, Z.; Gorfinkiel, J.D.; McEachran, R.P.; Brunger, M.J.; García, G. Cross-section calculations for positron scattering from pyrimidine over an energy range from 0.1 to 10000 eV. *Phys. Rev. A* **2013**, *88*, 062704. [[CrossRef](#)]
30. Sinha, N.; Sahoo, A.K.; Antony, B. Positron scattering from pyridine and pyrimidine. *J. Phys. Chem. A* **2020**, *124*, 5147–5156. [[CrossRef](#)] [[PubMed](#)]
31. Blanco, F.; Ellis-Gibbings, L.; García, G. Screening corrections for the interference contributions to the electron and positron scattering cross sections from polyatomic molecules. *Chem. Phys. Lett.* **2016**, *645*, 71–75. [[CrossRef](#)]
32. Blanco, F.; García, G. Interference effects in the electron and positron scattering from molecules at intermediate and high energies. *Chem. Phys. Lett.* **2015**, *635*, 321–327. [[CrossRef](#)]
33. Burke, P.G. *R-Matrix Theory of Atomic Collisions*; Springer: Berlin/Heidelberg, Germany, 2011.
34. Blanco, F.; García, G. Screening corrections for calculation of electron scattering from polyatomic molecules. *Phys. Lett. A* **2003**, *317*, 458–462. [[CrossRef](#)]
35. Blanco, F.; García, G. Screening corrections for calculation of electron scattering differential cross sections from polyatomic molecules. *Phys. Lett. A* **2004**, *330*, 230–237. [[CrossRef](#)]
36. Franz, J.; Gianturco, F.A. Low-energy positron scattering from gas-phase pyrimidine: A quantum treatment of the dynamics and a comparison with experiments. *Phys. Rev. A* **2013**, *88*, 042711. [[CrossRef](#)]
37. Fabrikant, I.I. Long-range effects in electron scattering by polar molecules. *J. Phys. B At. Mol. Opt. Phys.* **2016**, *49*, 222005. [[CrossRef](#)]

38. Itikawa, Y. The Born closure approximation for the scattering amplitude of an electron-molecule collision. *Theor. Chem. Acc.* **2000**, *105*, 123. [CrossRef]
39. Bederson, B.; Kieffer, L.J. Total Electron—Atom Collision Cross Sections at Low Energies—A Critical Review. *Rev. Mod. Phys.* **1971**, *43*, 601. [CrossRef]
40. Gilbert, S.J.; Kurz, C.; Greaves, R.G.; Surko, C.M. Creation of a monoenergetic pulsed positron beam. *Appl. Phys. Lett.* **1997**, *70*, 1944. [CrossRef]
41. Sullivan, J.P.; Jones, A.; Caradonna, P.; Makochekeanwa, C.; Buckman, S.J. A positron trap and beam apparatus for atomic and molecular scattering experiments. *Rev. Sci. Instrum.* **2008**, *79*, 113105. [CrossRef]
42. Sullivan, J.P.; Makochekeanwa, C.; Jones, A.; Caradonna, P.; Slaughter, D.S.; Machacek, J.; McEachran, R.P.; Mueller, D.W.; Buckman, S.J. Forward angle scattering effects in the measurement of total cross sections for positron scattering. *J. Phys. B At. Mol. Opt. Phys.* **2011**, *44*, 035201. [CrossRef]
43. Zecca, A.; Chiari, L.; García, G.; Blanco, F.; Trainotti, E.; Brunger, M.J. Total cross sections for positron and electron scattering from pyrimidine. *J. Phys. B At. Mol. Opt. Phys.* **2010**, *43*, 215204. [CrossRef]
44. Palihawadana, P.; Boadle, R.; Chiari, L.; Anderson, E.K.; Machacek, J.R.; Brunger, M.J.; Buckman, S.J.; Sullivan, J.P. Positron scattering from pyrimidine. *Phys. Rev. A* **2013**, *88*, 01271. [CrossRef]
45. Brunger, M.J.; Buckman, S.J.; Ratnavelu, K. Positron scattering from molecules: An experimental cross section compilation for positron transport studies and benchmarking theory. *J. Phys. Chem. Ref. Data* **2017**, *46*, 023102. [CrossRef]
46. Sahgal, V.; Bharadvaja, A.; Baluja, K.L. Positron-induced scattering of acetone from 0.1 eV to 5 keV. *J. Phys. B At. Mol. Opt. Phys.* **2021**, *54*, 075202. [CrossRef]
47. Sahgal, V.; Bharadvaja, A.; Baluja, K.L.; Arora, A.K.; Gupta, K.K. Positron-induced scattering from pentane isomers beyond ionization threshold. *Eur. Phys. J. D* **2021**, *75*, 259. [CrossRef]
48. Arora, A.K.; Sahgal, V.; Bharadvaja, A.; Baluja, K.L. Positron-impact scattering off 1-1 C₂H₂F₂ from 0.1 eV to 4 keV. *Phys. Rev. A* **2021**, *104*, 022816. [CrossRef]
49. Fedus, K.; Karwasz, G.P. Binary-encounter dipole Model for positron-impact direct ionization. *Phys. Rev. A* **2019**, *100*, 062702. [CrossRef]
50. Kim, Y.-K. Scaled Born cross sections for excitations of H₂ by electron impact. *J. Chem. Phys.* **2007**, *126*, 064305. [CrossRef]
51. Gianturco, F.A.; Lucchese, R.R.; Sanna, N.; Talamo, A. A generalized single centre approach for treating electron scattering from polyatomic molecules. In *Electron Collisions with Molecules, Clusters, and Surfaces*; Springer: Boston, MA, USA, 1994; pp. 71–86. [CrossRef]
52. Gianturco, F.A.; Sanna, N. SCELIB: A parallel computational library of molecular properties in the single-center expansion approach. *Comput. Phys. Commun.* **2000**, *128*, 139. [CrossRef]
53. Zhang, R.; Faure, A.; Tennyson, J. Electron and positron collisions with polar molecules: Studies with the benchmark water molecule. *Phys. Scr.* **2009**, *80*, 015301. [CrossRef] [PubMed]
54. Faisal, F.H.M. Electron-molecule interactions. I. Single-centre wave functions and potentials. *J. Phys. B At. Mol. Opt. Phys.* **1970**, *3*, 636. [CrossRef]
55. Burke, P.G.; Sinfailam, A.L. Electron-molecule interactions. II. Scattering by closed-shell diatomic molecules. *J. Phys. B At. Mol. Opt. Phys.* **1970**, *3*, 641. [CrossRef]
56. Perdew, J.P.; Zunger, A. Self-interaction correction to density-functional approximations for many-electron systems. *Phys. Rev. B* **1981**, *23*, 5048. [CrossRef]
57. Gianturco, F.A.; Jain, A. The theory of electron scattering from polyatomic molecules. *Phys. Rep.* **1986**, *143*, 347–425. [CrossRef]
58. Chang, E.S.; Fano, U. Theory of Electron-Molecule Collisions by Frame Transformations. *Phys. Rev. A* **1972**, *6*, 173. [CrossRef]
59. Bray, I.; Abdurakhmanov, I.B.; Bailey, J.J.; Bray, A.W.; Fursa, D.V.; Kadyrov, A.S.; Rawlins, C.M.; Savage, J.S.; Stelbovics, A.T.; Zammit, M.C. Convergent close-coupling approach to light and heavy projectile scattering on atomic and molecular hydrogen. *J. Phys. B At. Mol. Opt. Phys.* **2017**, *50*, 202001. [CrossRef]
60. Kadyrov, A.S.; Bray, I. Recent progress in the description of positron scattering from atoms using the convergent close-coupling theory. *J. Phys. B At. Mol. Opt. Phys.* **2016**, *49*, 222002. [CrossRef]
61. Utamuratov, R.; Kadyrov, A.S.; Fursa, D.V.; Zammit, M.C.; Bray, I. Two-center close-coupling calculations of positron-molecular-hydrogen scattering. *Phys. Rev. A* **2015**, *92*, 032707. [CrossRef]
62. Klar, H. Threshold ionisation of atoms by positrons. *J. Phys. B At. Mol. Opt. Phys.* **1981**, *14*, 4165–4170. [CrossRef]
63. Kim, Y.-K.; Rudd, M.E. Binary-encounter-dipole model for electron-impact ionization. *Phys. Rev. A* **1994**, *50*, 3954. [CrossRef]
64. Johnson, R.D., III (Ed.) Computational Chemistry Comparison and Benchmark Database, NIST Standard Reference Database Number 101, Release 21, August 2020. Available online: <http://cccbdb.nist.gov/> (accessed on 20 December 2022). [CrossRef]
65. Frisch, M.J.; Trucks, G.W.; Schlegel, H.B.; Scuseria, G.E.; Robb, M.A.; Cheeseman, J.R.; Montgomery, J.A., Jr.; Vreven, T.; Kudin, K.N.; Burant, J.C.; et al. *GAUSSIAN 03*; Gaussian, Inc.: Wallingford, UK, 2003. [CrossRef]
66. Sanna, N.; Baccarelli, I.; Morelli, G. SCELlib3.0: The new revision of SCELlib, the parallel computational library of molecular properties in the Single Center Approach. *Comput. Phys. Commun.* **2009**, *180*, 2544–2549. [CrossRef]
67. Sanna, N.; Gianturco, F.A. Differential cross sections for electron/positron scattering from polyatomic molecules. *Comput. Phys. Commun.* **1998**, *114*, 142–167. [CrossRef]

68. Jones, D.B.; Bellm, S.M.; Blanco, F.; Fuss, M.; García, G.; Limão-Vieira, P.; Brunger, M.J. Differential cross sections for the electron impact excitation of pyrimidine. *J. Chem. Phys.* **2012**, *137*, 074304. [[CrossRef](#)]
69. Fischer, G.; Cai, Z.-L.; Reimers, J.R.; Wormell, P. Singlet and Triplet Valence Excited States of Pyrimidine. *Phys. Chem. A* **2003**, *107*, 3093. [[CrossRef](#)]
70. Bassi, M.; Bharadvaja, A.; Baluja, K.L. A study of electron scattering from 1-1 $C_2H_2F_2$ from 0.1 eV to 5 keV. *Eur. Phys. J. D* **2019**, *74*, 232. [[CrossRef](#)]
71. Luthra, M.; Garkoti, P.; Goswami, K.; Bharadvaja, A.; Baluja, K.L. Electron impact cross-sections of tetraethyl silicate. *Plasma Sources Sci. Technol.* **2022**, *31*, 095013. [[CrossRef](#)]
72. Kaur, S.; Bharadvaja, A.; Baluja, K.L. Electron interactions with AlF. *Eur. Phys. J. D* **2022**, *76*, 176. [[CrossRef](#)]
73. Meltzer, T.; Tennyson, J.; Mašin, Z.; Zammit, M.C.; Scarlett, L.H.; Fursa, D.V.; Bray, I. Benchmark calculations of electron impact electronic excitation of the hydrogen molecule. *J. Phys. B At. Mol. Opt. Phys.* **2020**, *53*, 145204. [[CrossRef](#)]
74. Machacek, J.R.; McEachran, R.P. Partial wave analysis for folded differential cross sections. *J. Phys. B At. Mol. Opt. Phys.* **2018**, *51*, 065007. [[CrossRef](#)]
75. Dickinson, A.J. Differential cross sections for electron scattering by strongly polar molecules. *J. Phys. B* **1977**, *10*, 967. [[CrossRef](#)]
76. Bug, M.U.; Woon, Y.B.; Rabus, H.; Villagrasa, C.; Meylan, S.; Rosenfeld, A.B. An electron-impact cross section data set (10 eV–1 keV) of DNA constituents based on consistent experimental data: A requisite for Monte Carlo simulations. *Radiat. Phys. Chem.* **2017**, *130*, 459–479. [[CrossRef](#)]
77. Linert, I.; Dampc, M.; Mielewska, B.; Zubek, M. Cross sections for ionization and ionic fragmentation of pyrimidine molecules by electron collisions. *Eur. Phys. J. D* **2012**, *66*, 20. [[CrossRef](#)]
78. Champion, C.; Quinto, M.A.; Weck, P.F. Electron- and proton-induced ionization of pyrimidine. *Eur. Phys. J. D* **2015**, *69*, 127. [[CrossRef](#)]
79. Garkoti, P.; Luthra, M.; Goswami, K.; Bharadvaja, A.; Baluja, K.L. The Binary-Encounter-Bethe Model for Computation of Singly Differential Cross Sections Due to Electron-Impact Ionization. *Atoms* **2022**, *10*, 60. [[CrossRef](#)]
80. Charlton, M.; Humberston, J.W. *Positron Physics*; Cambridge University Press: Cambridge, UK, 2001. [[CrossRef](#)]
81. Chiari, L.; Zecca, A.; Girardi, S.; Trainotti, E.; García, G.; Blanco, F.; McEachran R.P.; Brunger, M.J. Positron scattering from O_2 . *J. Phys. B At. Mol. Opt. Phys.* **2012**, *45*, 215206. [[CrossRef](#)]
82. Luthra, M.; Goswami, K.; Arora, A.K.; Bharadvaja, A.; Baluja, K.L. Mass Spectrometry-Based Approach to Compute Electron-Impact Partial Ionization Cross-Sections of Methane, Water and Nitromethane from Threshold to 5 keV. *Atoms* **2022**, *10*, 74. [[CrossRef](#)]
83. Goswami, K.; Luthra, M.; Bharadvaja, A.; Baluja, K.L. Partial Ionization Cross Sections of Tungsten Hexafluoride Due to Electron Impact. *Atoms* **2022**, *10*, 101. [[CrossRef](#)]

Disclaimer/Publisher's Note: The statements, opinions and data contained in all publications are solely those of the individual author(s) and contributor(s) and not of MDPI and/or the editor(s). MDPI and/or the editor(s) disclaim responsibility for any injury to people or property resulting from any ideas, methods, instructions or products referred to in the content.